Frost flower aerosol effects on Arctic wintertime longwave cloud radiative forcing

Li Xu,[1] Lynn M. Russell,[1] Richard C. J. Somerville,[1] and Patricia K. Quinn[2]

[1] Frost flowers are clusters of highly saline ice crystals growing on newly formed sea ice or frozen lakes. Based on observations of particles derived from frost flowers in the Arctic, we formulate an observation-based parameterization of salt aerosol source function from frost flowers. The particle flux from frost flowers in winter has the order of $10^6\,\mathrm{m^{-2}\,s^{-1}}$ at the wind speed of $10\,\mathrm{m\,s^{-1}}$, but the source flux is highly localized to new sea ice regions and strongly dependent on wind speed. We have implemented this parameterization into the regional Weather Research and Forecasting model with Chemistry initialized for two wintertime scenarios. The addition of sea salt aerosol emissions from frost flowers increases averaged sea salt aerosol mass and number concentration and subsequent cloud droplet number. This change of cloud droplet number concentration increases downward longwave cloud radiative forcing through enhanced cloud optical depth and emissivity. The magnitude of this forcing of sea salt aerosols from frost flowers on clouds and radiation, however, contributes negligibly to surface warming in Barrow, Alaska, in the wintertime scenarios studied here.

Citation: Xu, L., L. M. Russell, R. C. J. Somerville, and P. K. Quinn (2013), Frost flower aerosol effects on Arctic wintertime longwave cloud radiative forcing, *J. Geophys. Res. Atmos.*, *118*, 13,282–13,291, doi:10.1002/2013JD020554.

1. Introduction

[2] The Arctic is a sensitive climate regime with Arctic surface temperatures projected to increase about twice as much as the global mean [*Houghton et al.*, 2001; *Arctic Climate Impact Assessment*, 2005]. Clouds play a critical role in the various feedbacks that operate in the Arctic. For instance, long-lived Arctic mixed-phase clouds, which consist of both liquid and ice water, have a large impact on radiative fluxes in the Arctic. These clouds persist for many days at a time, creating a self-sustaining resilient system through feedbacks among numerous local processes including the formation and growth of ice and cloud droplets, radiative cooling, turbulence, entrainment, and surface fluxes of heat and moisture [*Morrison et al.*, 2012]. Clouds exert a net warming effect on the Arctic climate system on average [*Intrieri et al.*, 2002], in contrast to lower latitudes where clouds have a net cooling effect. This difference is attributable to the absence of solar radiation during the polar winter and the high surface albedo of sea ice.

[3] Aerosol particles contribute to changing Arctic climate through the modification of cloud microphysical and radiative properties. Climate models currently include only sea salt from open water. Recent Antarctic studies provide evidence of large winter sources from neither open ocean nor transported sea salt from the midlatitudes but instead from wind-driven emissions in regions with newly formed ice [*Rankin and Wolff*, 2003]. *Simpson et al.* [2007] suggested that snow contaminated with sea salt on first-year sea ice may be a sea salt source, but there are large uncertainties in such analysis due to possible deficiencies in the use of satellite-passive microwave data associated with land contamination in coastal regions, low spatial resolution, and related issues. An alternative is that frost flowers may contribute to the high salt loading during winter and early spring in polar regions when young sea ice (e.g., nilas, leads) replaces open water near coastal sampling sites [*Rankin et al.*, 2000, 2002; *Rankin and Wolff*, 2003]. While *Roscoe et al.* [2011] found that frost flowers were very stable at high wind speeds up to $12\,\mathrm{m\,s^{-1}}$, this might have been because the laboratory conditions were not representative of the Arctic [*Fenger et al.*, 2013]. *Yang et al.* [2008] suggested blowing snow as a potential aerosol source, while *Nghiem et al.* [2012] challenged this view for the Arctic.

[4] Frost flowers are clusters of high-saline ice crystals growing on newly formed sea ice or frozen lakes. They wick brine from the surface of sea ice [*Domine et al.*, 2005]. They typically last about a few days after the initial formation and then are buried by snow, sublimate as sea ice grows thicker [*Style and Worster*, 2009], or are blown away by wind that lofts the nonvolatile fraction into the atmosphere as aerosol particles [*Perovich and Richter-Menge*, 1994]. *Rankin et al.* [2000] showed that there is close agreement in the sulfate/sodium ratio between one frost flower sample from the Weddell Sea and aerosol collected in winter at the British Antarctic Survey station Halley Bay in Antarctica. This agreement suggests that frost flowers are responsible for the majority of sea salt aerosol produced within the

---

[1]Scripps Institution of Oceanography, University of California, San Diego, La Jolla, California, USA.
[2]PMEL, NOAA, Seattle, Washington, USA.

Corresponding author: L. M. Russell, Scripps Institution of Oceanography, University of California, San Diego, La Jolla, CA 92093, USA. (lmrussell@ucsd.edu)

sea ice zone in winter in polar regions. Furthermore, *Rankin and Wolff* [2003] estimated that frost flowers contribute at least 60% of the total sea salt arriving at Halley Bay during a yearlong study of size-segregated aerosol composition. Aerosol particle compositions consistent with frost flowers have also been found in the Arctic [*Beaudon and Moore*, 2009].

[5] Although frost flowers are believed to be a major source of sea salt aerosol during winter and early spring in polar regions [*Rankin et al.*, 2000, 2002; *Rankin and Wolff*, 2003], the aerosol particle formation mechanism from frost flowers is not well established. Mechanical breakage of frost flowers is postulated as one major possible mechanism by which frost flowers produce aerosol particles [*Alvarez-Aviles et al.*, 2008]. Two other possible mechanisms include brine blown from the frost flower structure directly and particles produced by pressurization of the brine channel during the cooling process of frost flowers [*Alvarez-Aviles et al.*, 2008]. *Obbard et al.* [2009] suggest that blowing snow salinated by contact with frost flowers may contribute atmospheric sea salt aerosol particles.

[6] Global models include aerosol production from frost flowers to study their effects on oxidants [*Piot and von Glasow*, 2009; *Zhao et al.*, 2008] and on the Last Glacial Maximum [*Mahowald et al.*, 2006]. These models use a sea salt source function from open water to represent the aerosols generated from frost flowers as a necessarily rough approximation. Nevertheless, the addition of frost flowers was shown to improve predicted ozone concentrations [*Piot and von Glasow*, 2009] because frost flowers are believed to release bromine, a reactive catalyst responsible for ozone destruction.

[7] In this study, we derive an observationally based parameterization to estimate sea salt production from frost flowers. We use the potential frost flower (PFF) coverage proposed by *Kaleschke et al.* [2004] in conjunction with the statistical relationship between the ocean-derived factor (i.e., a factor composed of organic hydroxyl groups and closely tied with organic and inorganic seawater components [*Russell et al.*, 2010]) and wind speed observed for Barrow by *Shaw et al.* [2010] to formulate the total aerosol source flux (F), following, by convention, the exponential relationship ($\log F = a\, U + c$) [*Nilsson et al.*, 2001; *Geever et al.*, 2005]. This parameterization is introduced in section 2.1. The regional model (Weather Research and Forecasting model with Chemistry (WRF-Chem)), described in section 2.2, is used to compare this parameterization to measurements at Barrow and to assess the influence of this "missing" sea salt-containing wintertime particle source on clouds and their longwave radiation. The results are presented in section 3 followed by discussion and conclusions in section 4.

2. Methodology

2.1. Parameterization of Sea Salt Aerosol Source From Frost Flower

[8] In this study, we proposed and evaluated a physically based parameterization of sea salt particles from frost flowers. First, we adopted the algorithm outlined in *Kaleschke et al.* [2004] to identify the potential regions in which frost flowers can grow. Following the formulation of sea salt aerosol production from breaking waves in open water [*Martensson*

*et al.*, 2003], we proposed a general form of the sea salt particle flux (F) from frost flowers as follows:

$$\frac{\mathrm{d}F}{\mathrm{d}\log(D_p)} = \frac{\Phi \cdot e^{-\frac{[\log(D_p)-\log(D_g)]^2}{2\log(\sigma_g)^2}}}{\sqrt{2\pi}\log(\sigma_g)} \cdot \mathrm{PFF}\,(\mathrm{m}^2\mathrm{s}^{-1}), \qquad (1)$$

where D_p stands for particle diameter, D_g and σ_g represent geometric diameter and standard deviation of aerosol size distribution, Φ is the total particle number flux produced per surface area of frost flowers per second, and PFF stands for the potential frost flower coverage defined and parameterized in *Kaleschke et al.* [2004]. Following *Geever et al.* [2005], we formulated an exponential relationship between the particle flux and wind speed (u) using the relationship between the ocean-derived factor and wind speed identified in *Shaw et al.* [2010] and assuming that the ocean-derived particles are released from frost flowers grown in sea ice in winter,

$$\Phi = e^{0.24u - 0.84}. \qquad (2)$$

[9] We adopted the magnitude of the source flux of $10^6\,\mathrm{m}^2\,\mathrm{s}^{-1}$ [*Geever et al.*, 2005], since *Rankin et al.* [2000] suggested the salt production from frost flowers has a similar magnitude to that from open water. *Kaleschke et al.* [2004] introduced PFF as a proxy for predicting the surface area from which frost flowers may form on sea ice using a one-dimensional thermodynamic model of sea ice and the frost flower growth. We assumed that sea salt aerosols emitted from frost flowers follow a lognormal size distribution with a geometric diameter (D_g) of 0.15 μm and a standard deviation (σ_g) of 1.9. The size distribution we adopted here for the aerosols generated from frost flowers was based on observed accumulation mode aerosol size distributions at Barrow from November 2008 to February 2009 (A. Jefferson, personal communication, 2013). The daily submicron aerosol size distribution in Barrow is measured by a Scanning Mobility Particle Sizer (SMPS) with 70 diameter and number concentration channels, and the diameter ranges from 8.7 nm to 984.6 nm. Use of these observed size distributions assumes that the measured aerosol was primarily sea salt in the Arctic winter (shown in Figure 1a) [*Shaw et al.*, 2010]. This geometric diameter is consistent with the value (0.17 μm) for high latitudes reported in *Heintzenberg et al.* [2000].

[10] Figure 1b shows the source flux (Φ) as a function of wind speed. The sea salt aerosol flux from frost flowers in winter is of the order of $1 \times 10^6\,\mathrm{m}^{-2}\,\mathrm{s}^{-1}$ at the wind speed of $1\,\mathrm{m}\,\mathrm{s}^{-1}$, increasing to $5 \times 10^6\,\mathrm{m}^{-2}\,\mathrm{s}^{-1}$ at $10\,\mathrm{m}\,\mathrm{s}^{-1}$. As suggested in *Alvarez-Aviles et al.* [2008] and *Shaw et al.* [2010], frost flowers are composed of distinct chemical compositions in different stages of growth and include contributions of organic constituents from seawater. It is noted that we use the composition of seawater to represent sea salt aerosols from frost flowers. This assumption is made because we have no information about the dependence of the aerosol source function on various parameters (including salinity, which varies substantially in frost flowers) [*Alvarez-Aviles et al.*, 2008]. However, we use an aerosol size distribution constrained by observations at Barrow to implicitly include the locally relevant range of parameters that affect the
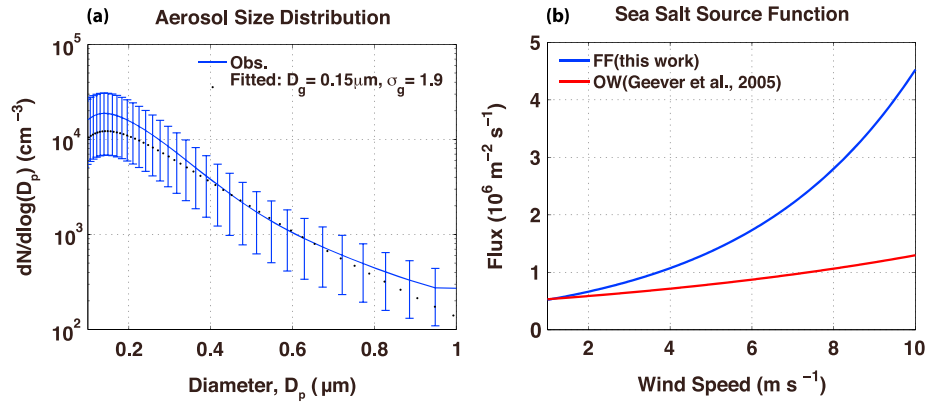
Figure 1. (a) Observed and fitted mean aerosol size distribution in Barrow, Alaska averaged during the period from November 2008 to February 2009; (b) sea salt number flux from frost flowers (FF) parameterized in this work (blue line) in comparison to that from open water (OW) proposed by *Geever et al*. [2005].

particle size of frost flower aerosols. In addition, frost flowers serve as the source of the carbohydrate-like organic components during Arctic winter [*Shaw et al*., 2010; *Bowman and Deming*, 2010]. They also serve as ice nuclei [*Christner et al*., 2008] to modify different types of clouds (e.g., ice clouds or mixed-phase clouds) in the Arctic. However, primary marine organic aerosols may change cloud droplet number less than sea salt because of their different surface, hygroscopic, and optical properties [*Ming and Russell*, 2001; *Randles et al*., 2004]. Previous laboratory-based measurements [*Fuentes et al*., 2011; *Moore et al*., 2011] and global modeling studies [*Westervelt et al*., 2012; *Gantt et al*., 2012] have shown that mixing marine organic compounds into sea salt solutions has a small influence on the prediction of cloud droplet number concentration and their associated cloud shortwave climate forcing, suggesting that neglecting organic mass in this work would cause only minimal changes in cloud longwave forcing, which are small relative to the large uncertainties associated with emission strength that are shown here.

2.2. WRF-Chem Model

[11] In this study, WRF-Chem version 3.4 was applied. Table 1 summarizes the WRF-Chem model configuration options used in this study. We incorporated the parameterization of sea salt particle production from frost flowers in the WRF-Chem model and adopted the option of fractional sea ice. By incorporating the open ocean fraction (i.e., 1 minus fractional sea ice), we modified the original sea salt source function from open water that only emits sea salt at the grid identified as a body of water using the binary land-sea mask (i.e., land = 1 and sea = 0). The usage of this binary land mask may result in the underestimation of sea salt aerosol generation in the polar regions, especially in winter. WRF-Chem was configured using one-way nested domains with grid spaces of 30 km and 6 km shown in Figure 2a. The coarsest grid (Domain 1) extended approximately from latitudes 60°N to 80°N and from 175°W to 140°W, covering northern Alaska, the Bering Strait, and the Beaufort Sea as shown in Figure 2a. This area includes young coastal ice rivers and lakes as well as open oceans and is close to Barrow where frost flower growth was identified by *Shaw et al*. [2010]. Domain 2 was centered near Barrow. Both domains extended 27 layers in the vertical, from the surface to 100 hPa, with finer resolution near the surface.

[12] The first scenario for simulation was chosen as the period of 31 January 2009 00:00 UTC through 2 February 2009 00:00 UTC. This period included the winter maximum of sodium and chloride measured in Barrow, Alaska [*Shaw et al*., 2010]. These high salt concentrations as well as positive matrix factorization of the measurements of organic particle composition performed by *Shaw et al*. [2010] indicate that the ocean-derived factor was substantially larger during this 2 day period than factors attributed to other sources such as industrial, shipping, and biomass combustion from Siberia. Because the frost flower source was substantial, this period provided an appropriate case study of the climate effects of frost flowers during the Arctic winter with minimal influence from anthropogenic aerosols transported from the midlatitudes.

[13] Equation (1) was used to calculate aerosol source fluxes from frost flowers in submicron aerosol size bins with the upper diameter of the bins ranging from 0.15 to 1.25 μm in the Model for Simulating Aerosol Interactions and Chemistry aerosol module of the WRF-Chem model. The preprocessed PFF was calculated using satellite-derived sea ice fraction from 0.5 × 0.5 degree gridded National Snow and Ice Data Center Special Sensor Microwave/Imager passive microwave data [*Maslanik and Stroeve*, 1999] along with the 1 × 1 degree gridded National Centers for Environmental Prediction (NCEP) reanalysis surface air temperature [*Kalnay et al*., 1996]. Using a frost flower lifetime of up to 5 days, the PFF coverage for each day was computed by integrating the values from the current day and four previous

Table 1. Configuration Options Employed in the WRF-Chem in This Study

Atmospheric Process	Model Options	Reference
Gas phase chemistry	Carbon Bond Mechanism version Z (CBMZ)	*Zaveri and Peters* [1999]
Aerosol chemistry	MOSAIC eight bins	*Zaveri et al*. [2008]
Surface layer	Monin-Obukov	*Janjic* [1996]
Land surface	Noah Land Surface Model (LSM)	*Chen and Dudhia* [2001]
Boundary layer	YSU	*Hong and Lim* [2006]
Cloud microphysics	LIN	*Lin et al*. [1983]
Longwave radiation	RRTMG	*Iacono et al*. [2008]
Shortwave radiation	Goddard	*Chou et al*. [1998]
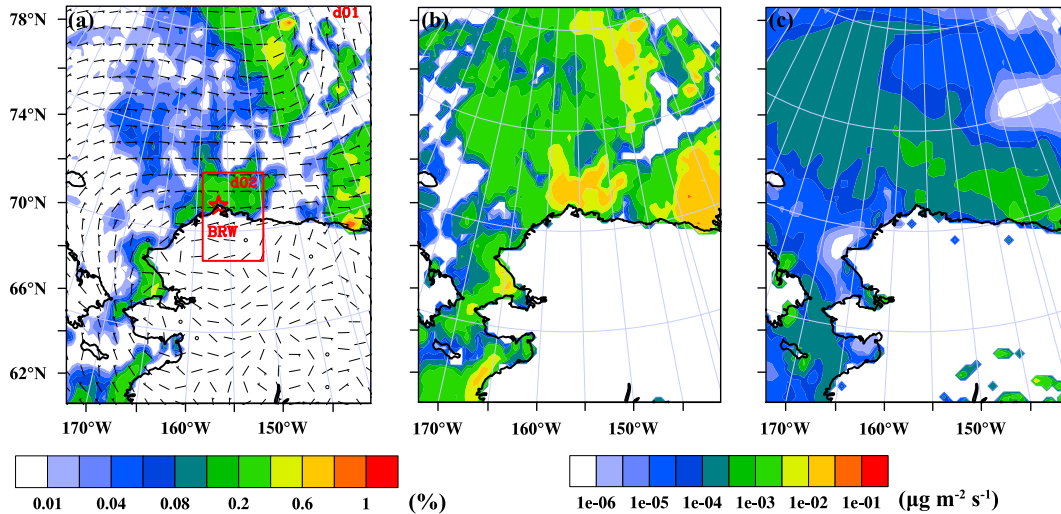
Figure 2. (a) Daily averaged potential frost flower coverage (%) overlaid with daily average wind fields, submicron sea salt aerosol emission (b) from frost flowers (FF) and (c) from open water (OW) on 1 February 2009. The "d01" in red represents Domain 1, while the "d02" in red and rectangular box represents Domain 2. The star stands for the location of Barrow (i.e., BRW).

days, which then served as an input variable for the daily fractional coverage of frost flowers in WRF-Chem. Note that the largest difference in the PFF coverage is less than 10% when the model integration time (i.e., the lifetime of frost flowers) varies from 1 day to 5 days at surface air temperature −40°C shown in *Kaleschke et al.* [2004]. Initial and lateral boundary conditions for meteorological variables were obtained from the NCEP global forecast system final (FNL) operational analyses. In this study, we designed two numerical experiments: one case includes sea salt only from open water (hereafter referred to as OW), while the other includes salt source functions from both open water and frost flowers (hereafter referred to as FF). This study used the prescribed sea ice fraction provided from FNL, so there is no feedback of albedo on sea ice amount.

[14] For this wintertime scenario, two different sets of aerosol particle concentrations were used for the initial and boundary conditions: one representing clean marine conditions and the other representing polluted conditions. For the clean conditions, submicron particle mass consisting of $0.89\,\mu g\,m^{-3}$ (or $0.04\,\mu mol\,m^{-3}$) of sodium and $1.9\,\mu g\,m^{-3}$ (or $0.05\,\mu mol\,m^{-3}$) of chloride was used, based on observed concentrations at Barrow on 31 January 2009. For the polluted conditions, the same sodium and chloride concentrations were used as in the clean conditions, but the sulfate, nitrate, ammonium, organic carbon, elemental carbon, and other inorganic aerosols (e.g., calcium, magnesium, and potassium cation) were initialized as 1.5, 0.14, 0.4, 0.86, 0.1, and $0.84\,\mu g\,m^{-3}$, respectively, using typical springtime concentrations reported by *Shaw et al.* [2010]. We used these polluted concentrations to mimic possible influence of anthropogenic aerosols transported from the midlatitudes on the pristine Arctic. An exponential decrease of aerosol concentration with altitude was assumed. The model spin-up time was 24 h. The simulation starting from 00:00 UTC on 1 February 2009 was used in the analysis. The base clean condition on 1 February was the main focus in the analysis. In addition, we also examined the influence of sea salts from frost flowers under a less humid ambient

environment initialized for the clean marine condition. A somewhat less humid day (11 January 2009), with an averaged relative humidity of 73% over Domain 1, was chosen to contrast with 1 February 2009 which had an averaged relative humidity of about 80%. The results on 11 January 2009 were integrated from 10 January 2009.

3. Results

[15] The extent to which frost flowers affect cloud properties and consequent longwave cloud radiative forcing in the polar regions depends on how widespread regions of new sea ice are. Figure 2a shows the potential frost flower coverage calculated using the method of *Kaleschke et al.* [2004] on 1 February 2009 for Domain 1. The highest potential frost flowers coverage, about 1%, is found in coastal leads and the Beaufort Sea. Note the PFF is regarded as a maximum frost flower area for a given set of conditions. As discussed in *Kaleschke et al.* [2004], a minimum frost flower area cannot be estimated due to insufficient understanding of the initial formation and growth of frost flowers as well as decay processes.

[16] For new ice to form, open water must be present which occurs most often when winds are offshore, creating a shore lead. However, for aerosols generated from frost flowers to be blown inland, the wind direction must change to blow onshore. The wind conditions shown in Figure 2a are favorable to generate salt particles from frost flowers and transport it inland. The daily averaged sea salt emission from frost flowers and open water are shown in Figures 2b and 2c. The daily average sea salt emission from frost flowers in Domain 1 is about $2.4 \times 10^{-3}\,\mu g\,m^{-2}\,s^{-1}$, similar in magnitude with that from open water, $3.3 \times 10^{-3}\,\mu g\,m^{-2}\,s^{-1}$, resulting in roughly a factor of 2 higher total sea salt flux from the FF case (which includes FF and OW sea salt) compared to the OW case. Moreover, the salt emission distribution over Domain 1 is highly tied to the distribution of potential frost flower coverage, which is distinct from the salt emission distribution from open water.
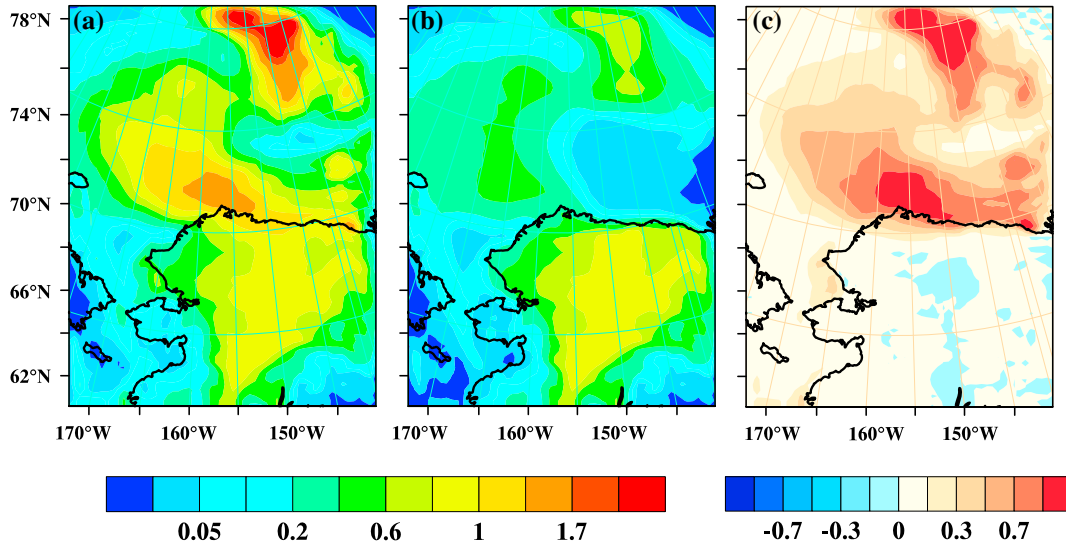
Figure 3. Daily averaged sodium concentration from the (a) FF and (b) OW cases along with (c) their absolute difference. The unit is $\mu g\,m^{-3}$.

[17] Figures 3a–3c show simulated daily averaged sodium aerosol concentration from FF and OW cases along with the absolute difference. The largest concentration of sodium-containing particles is close to source regions where the potential frost flower coverage is high. The lower concentrations over land result from the longer distance from the ocean sources. The highest enhancement of sodium concentration due to the addition of sea salt aerosols from frost flowers is up to a factor of 2 compared to the OW case in accordance with the higher emission from the FF case. The modeled daily averaged submicron sodium aerosol concentration in Barrow from the FF case is around $1.5\,\mu g\,m^{-3}$ (Table 2),

close to the observed value of $1.3\,\mu g\,m^{-3}$ [*Shaw et al.*, 2010]. The OW case underestimates the submicron sodium aerosol in Barrow by about 72%. The difference in total aerosol number concentration between the FF and OW cases shows a similar pattern to that of sea salt aerosol mass concentrations (not shown). The difference in the modeled sodium concentration ranges from 10% to 40% when using Domain 1 averaged values instead of interpolated values at point Barrow (Table 2).

[18] The activation of aerosols to form cloud droplets is estimated in this study using Köhler theory following the parameterization of *Abdul-Razzak and Ghan* [2002]. The

Table 2. Daily Averaged Modeled and Observed Aerosols, Cloud Properties, and Radiative Fluxes in Barrow Summarized on 1 February and 11 January 2009[a]

	FF						OW			
	1 Feb[b]				11 Jan[c]		1 Feb[b]			
	Base	2 × FF	0.5 × FF	Polluted	Base	0.1 × FF	Base	Polluted	11 Jan[c]	Observed[d]
Na Conc.[e] ($\mu g\,m^{-3}$)	1.45 (1.18)	2.54 (2.12)	0.91 (0.70)	1.45 (1.18)	13.95 (10.17)	2.20 (1.79)	0.37 (0.23)	0.37 (0.23)	0.90 (0.86)	1.30 (0.01–3.50)
Column-integrated cloud droplet number[f] (# cm^{-2})	169	185	163	257	26	25	154	222	25	-
Precipitation (mm)	0.85	0.85	0.85	0.85	0.15	0.15	0.85	0.85	0.15	1.85 (0.24)
All-sky longwave (LW) downward flux at surface (W m^{-2})	138.85	138.84	138.84	138.96	141.48	141.42	138.82	138.96	141.63	155.93 (150.17)
Clear-sky, LW downward flux at surface (W m^{-2})	136.32	136.33	136.32	136.45	140.56	140.56	136.31	136.44	140.56	-
Downward cloud LW forcing at surface (W m^{-2})	2.53	2.51	2.52	2.51	0.92	0.86	2.51	2.52	1.07	-

[a]The values in Domain 2 are adopted.

[b]The label "Base" represents simulated results from the base clean condition, while the labels "2 × FF" and "0.5 × FF" represent simulated results from 2 times higher and lower sea salt aerosol emissions from frost flower on 1 February 2009, respectively. The label "Polluted" stands for the simulated results initialized with anthropogenic aerosols along with sea salt aerosols on 1 February 2009.

[c]The label "Base" represents simulated results from the base clean condition, while the label "0.1 × FF" represents simulated results from 10 times lower sea salt aerosol emissions from frost flower on 11 January 2009, respectively.

[d]The observed accumulation mode aerosol concentrations in Barrow with the diameter less than 1.25 μm are taken from *Shaw et al.* [2010], while other values are obtained from Atmospheric Radiation Measurement (ARM) best estimate data set [*Xie et al.*, 2010] for 1 February 2009 and 11 January 2009 (i.e., values in the parentheses), respectively. Note that since measurements were not taken on 11 January 2009, we compare to the range of Na concentrations for winter months (January to February) in 2009 from two sets of XRF Na analyses [*Shaw et al.*, 2010; *Quinn et al.*, 2009].

[e]The values outside the parentheses in the row of "Na Conc." are the ones interpolated to point Barrow, while those inside of the parentheses are values averaged over Domain 2.

[f]The column-integrated cloud droplet number is averaged over Domain 2.
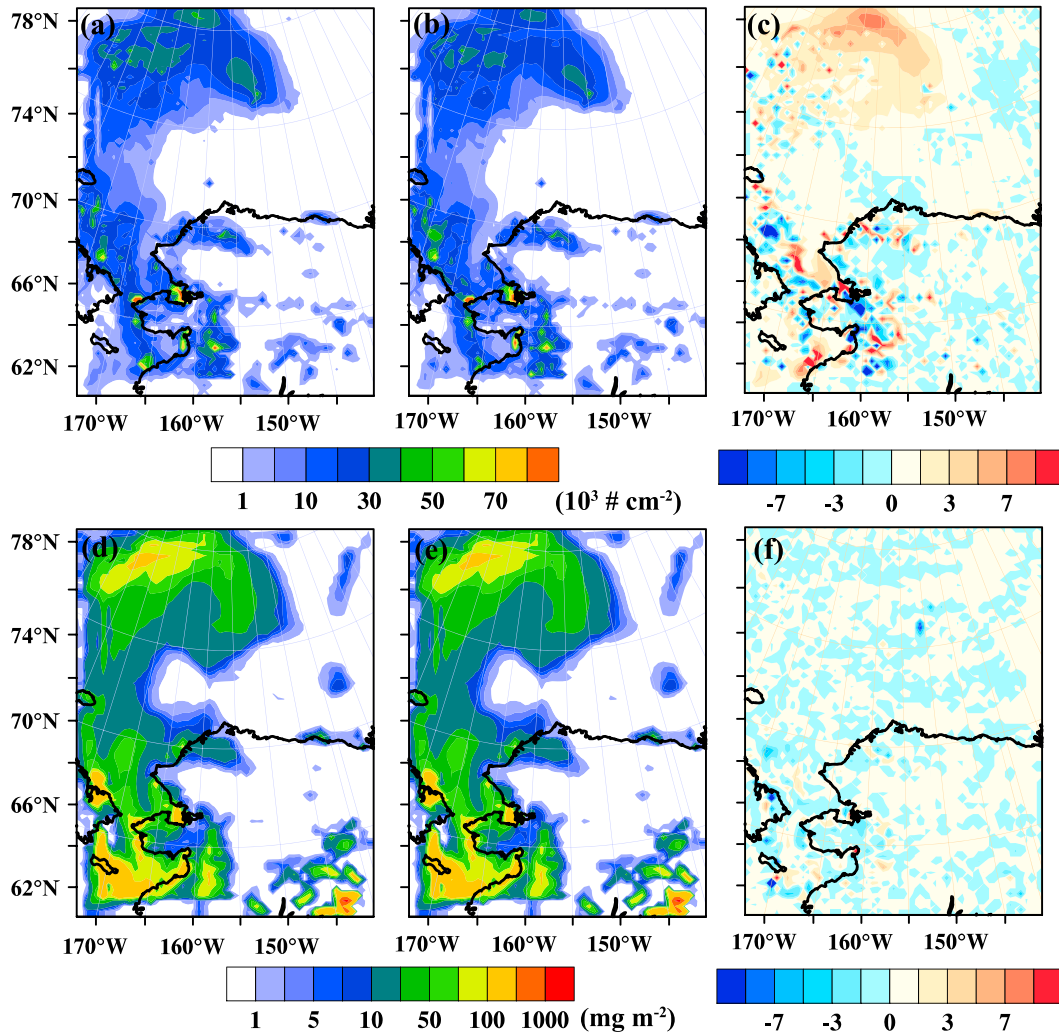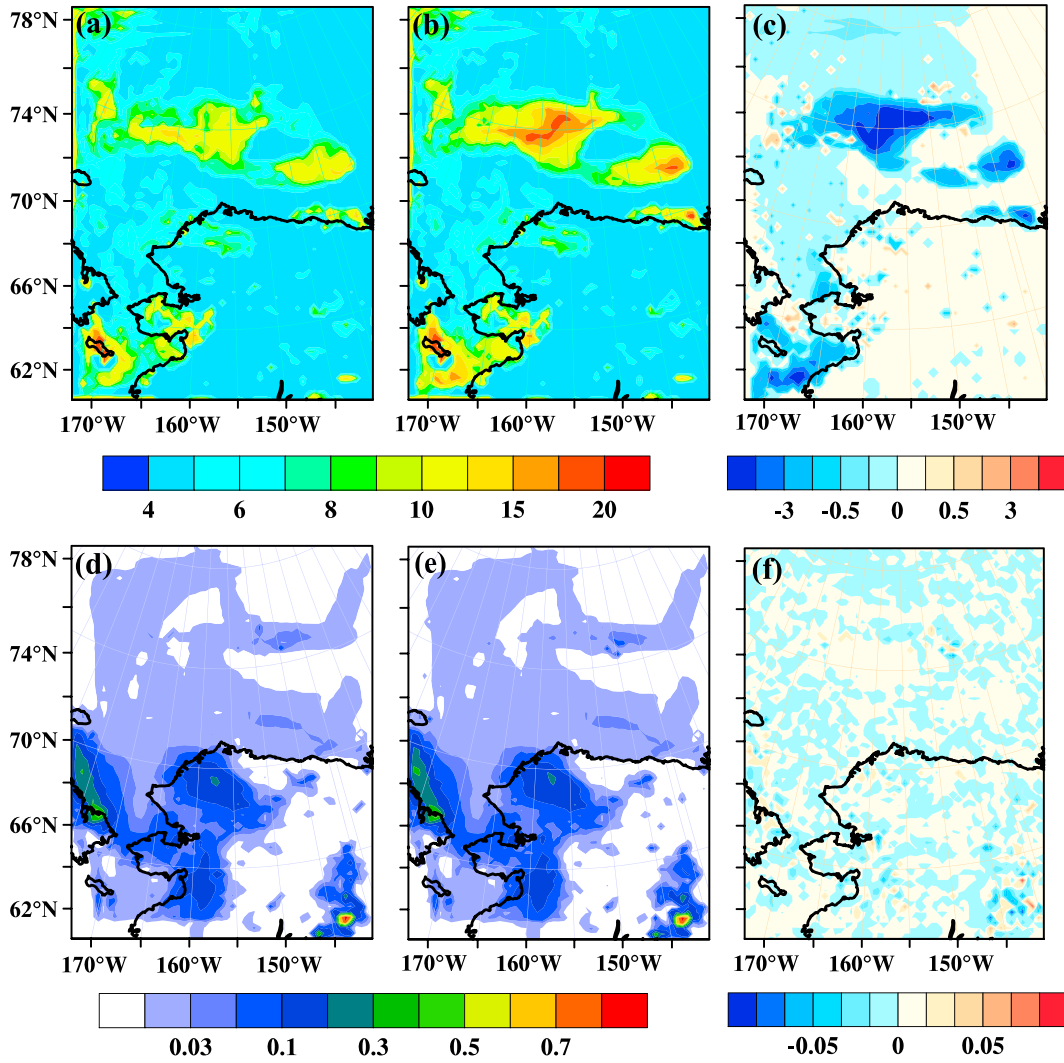
Figure 4. Daily averaged column-integrated cloud droplet number concentration from (a) FF and (b) OW and daily averaged column-integrated liquid water path below 1 km from (d) FF and (e) OW. The absolute difference between FF and OW in (c) cloud droplet number concentration and (f) liquid water path.

highest cloud droplet number concentrations are found over the Beaufort Sea, especially in the ~76–78°N latitude band where the largest difference in sodium concentration between FF and OW regions occurs (Figure 4). However, even with about a factor of 3 to 4 increase in the sodium mass or number concentration near the latitude band 76–78°N (Figure 3c), the increase of low-level cloud droplet number is only around 20% (Figure 4c) since cloud droplet number concentration (CDNC) is determined not only by aerosol particles but also by the local updraft velocity and available ambient water vapor. There is no observable increase in cloud droplet number concentration near the latitude band 70–72°N where the sodium aerosol mass concentration increases significantly (Figure 3c). That is because few clouds are present there as indicated from the low-level cloud liquid water path (Figures 4d–4f). Within the cloud, the cloud water content is similar for the FF and OW cases. No clear spatial pattern of modeled low-level cloud liquid water path is observed in contrast to that of sodium aerosol mass concentration and low-level cloud droplet number concentration.

[19] The increase in sea salt particle mass from frost flowers alters the radiative flux in the Arctic. Longwave warming dominates throughout the dark months in the Arctic. An increase in CDNC due to frost flowers is likely to increase downward longwave radiation by decreasing cloud droplet effective radius resulting in an increase in cloud optical depth and cloud emissivity. The spatial pattern of the decrease (increase) of cloud droplet effective radius (cloud optical depth) shown in Figures 5a (5d), 5b (5e), and 5c (5f) contributes to the change in downward longwave cloud forcing at the surface as illustrated in Figure 6. This change in longwave forcing is due to the addition of sea salt from frost flowers with an approximately $0.1 \, \mathrm{W \, m^{-2}}$ increase averaged over Domain 1 with up to $1 \, \mathrm{W \, m^{-2}}$ difference in the region of higher CDNC in the FF case. Table 2 summarizes modeled and observed sodium mass concentrations, cloud properties, and radiative fluxes at Barrow on 1 February 2009. Overall, compared to the OW case, the values predicted from the FF case are closer to observed values but the longwave radiative fluxes still underestimate the observations. *Porter et al.* [2011] showed WRF generally captures the Arctic energy budget estimated from reanalyses and satellite observations from the year 2000 to 2008 despite a few shortcomings. However, compared to European Centre for Medium-Range Weather Forecasts

Figure 5. Daily averaged cloud droplet effective radius (unit: μm) close to surface and column-integrated cloud optical depth below 1 km at the wave number band 10–350 cm^{-1} from the (a and d) FF and (b and e) OW cases along with (c and f) their absolute difference.
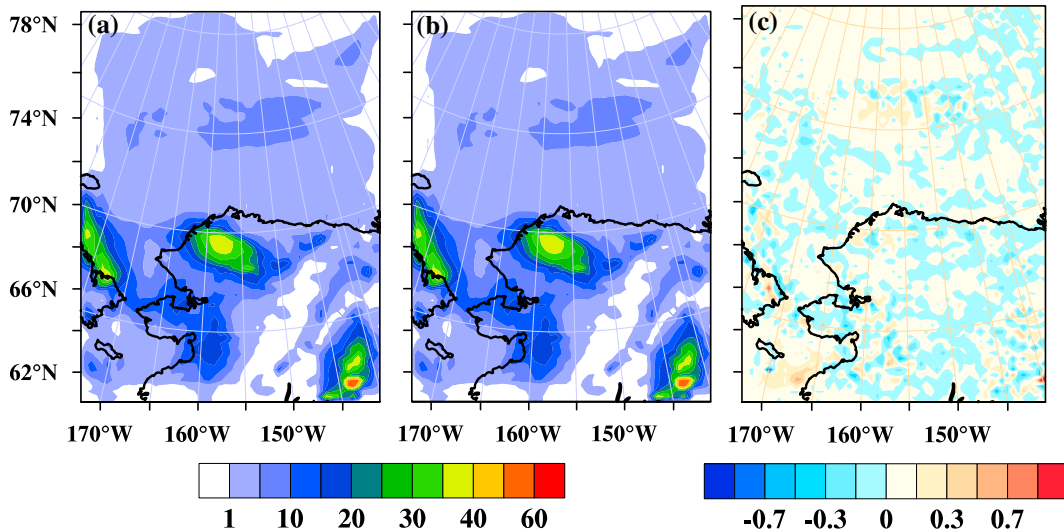
Figure 6. Daily averaged downward longwave cloud forcing at surface from the (a) FF and (b) OW cases along with (c) their absolute difference. The unit is W m^{-2}.
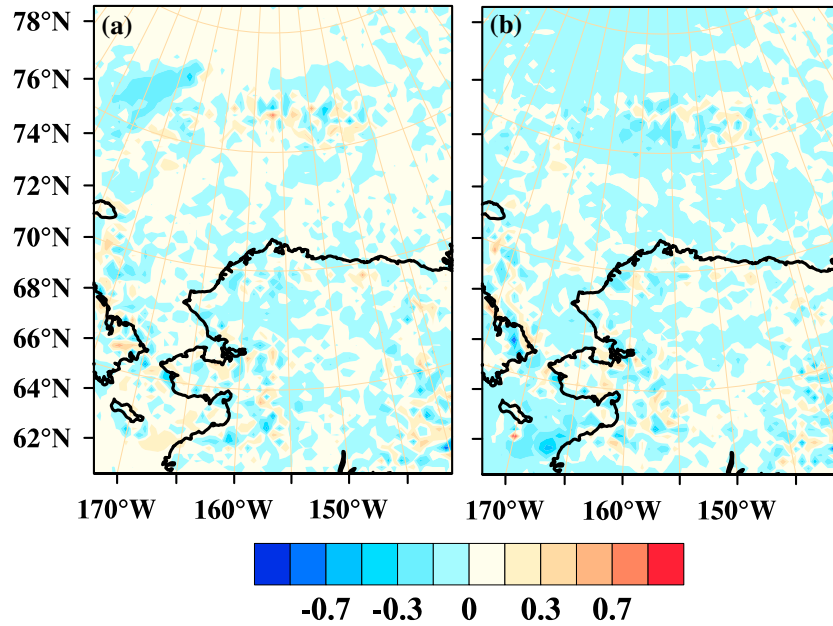
Figure 7. Daily averaged absolute difference in downward longwave cloud forcing at surface (a) between $2 \times FF$ and FF (i.e., $2 \times FF\text{-}FF$) and (b) between $0.5 \times FF$ and FF (i.e., $0.5 \times FF\text{-}FF$). The unit is $W\,m^{-2}$.

Interim Reanalysis data, the WRF model was found to be biased low for surface downwelling and upwelling longwave radiative fluxes ranging from 5 to 40 $W\,m^{-2}$ in winter months in the polar cap [*Porter et al.*, 2011], which is consistent with our results. The longwave warming due to the presence of clouds is estimated to be 2.53 $W\,m^{-2}$ from the FF case in contrast to 2.51 $W\,m^{-2}$ from the OW case, which is in accordance with the longwave cloud-forcing estimate of 3.4 $W\,m^{-2}$ at the surface suggested by *Lubin and Vogelmann* [2006]. This leads to about a 0.02 $W\,m^{-2}$ warming difference at Barrow due to the addition of sea salt emitted from frost flowers, which is equivalent to about a 1% increase in longwave cloud forcing. The effect of FF is small primarily due to the near absence of clouds. Hence, there is no significant modification of cloud properties even with the large increase of aerosol mass. In contrast, over the Beaufort Sea and Bering Strait, the longwave cloud forcing is enhanced up to 0.5 $W\,m^{-2}$ or by 5% due to the addition of salt sources from frost flowers. This enhancement is mainly ascribed to the corresponding decrease (increase) of cloud-effective radius (cloud droplet number concentrations) in these regions.

[20] In addition to the base case FF simulation, we conducted simulations with 2 times higher and lower sea salt emissions from frost flowers while keeping other fields the same as the clean condition. Figure 7a (7b) shows the daily averaged absolute difference in downward cloud longwave forcing at surface between case $2 \times FF$ and case FF (between case $0.5 \times FF$ and case FF), respectively. Overall, the changes in cloud longwave forcing at surface vary from roughly -1 to 1 $W\,m^{-2}$ for both sensitivity tests. The increase in sea salt aerosol emission from frost flowers leads to near-zero warming, while the decrease in emission contributes to slightly cooling. As shown in Table 2, doubling sea salt aerosols emitted from frost flowers increase sodium mass concentration by 75%, resulting in a 10% enhancement of column-integrated cloud droplet number concentration. The changes in precipitation and longwave radiative fluxes remain small, resulting in only a 0.8% increase

in downward longwave cloud forcing at the surface at Barrow. The changes in aerosols, clouds, and radiative fluxes also scale for the simulation with 2 times lower sea salt emission from frost flowers, indicating that longwave radiative fluxes and the resulting longwave cloud-forcing scale with the magnitude of the salt aerosol source from frost flowers for this wintertime study.

[21] Compared to the base clean conditions, both FF and OW cases in the polluted conditions predicted similar sodium mass concentration but higher cloud droplet number due to the activation of anthropogenic aerosols in addition to sea salt particles. The higher cloud droplet concentrations resulted in roughly 0.11–0.14 $W\,m^{-2}$ greater all-sky and clear-sky downward longwave cloud fluxes at the surface in Barrow compared to clean conditions for both OW and FF cases. The precipitation from both cases in the polluted condition is close to that in the clean condition. Some previous studies suggest that the precipitation could be suppressed under highly polluted ambient conditions [*Rosenfeld*, 1999; *Khain and Pokrovsky*, 2004; *Li et al.*, 2008], but there is no evidence for that at the low pollutant concentrations present in the Arctic regions.

[22] A simulation under less humid and clean conditions on 11 January 2009 was also conducted. The magnitude of positive longwave forcing at the surface was similar for the FF and OW cases even though simulated sodium aerosol concentrations at Barrow were much higher for the FF case (Table 2). The CDNC for the two cases was similar because of the limited available liquid water (i.e., less humidity). The potential frost flower coverage used in this simulation for 11 January 2009 is around 10% near coastal areas of Barrow. That is about a factor of 10 higher than the PFF shown in Figure 2a and results in a sodium aerosol mass concentration roughly 10 times higher than that calculated for the base clean condition on 1 February (Table 2). This magnitude of sodium concentration is much greater than the highest-observed submicron sodium concentration (i.e., around 3 $\mu g\,m^{-3}$) in the

wintertime (November to February) at Barrow from October 1997 to June 2008 [*Quinn et al.*, 2009]. A simulation with 10 times lower sea salt aerosol emissions from frost flowers (labeled as "$0.1 \times FF$" in Table 2) was performed while keeping other fields the same as the base less humid condition. With the lower aerosol emissions, the modeled sodium aerosol concentration from the less humid condition on 11 January 2009 falls within the observed sodium concentration ranges in Barrow for the winter months [*Shaw et al.*, 2010; *Quinn et al.*, 2009]. Cloud and radiative properties were scaled down correspondingly. Aerosol concentration is not only determined by emissions but also by transport and deposition. The production and transport of frost flower salt aerosols are not well understood. Still, this study helps explain the observations to some extent and qualitatively captures general features of physical and radiative processes involved in the interaction among sea salt aerosols, clouds, and longwave cloud forcing. More frost flower field measurements are required to fill in the knowledge gaps associated with the physical processes or mechanisms involved with frost flower decay and aerosol production.

4.   Discussion and Conclusions

[23]   The present study introduces an observation-based parameterization of sea salt mass concentration from frost flowers during the Arctic winter. The sea salt particle emissions from frost flowers were found to have a magnitude similar to or higher than that from open water during winter in regions downwind of new sea ice. The salt particle source from frost flowers was incorporated in the WRF-Chem model. We have shown that open water sources of sea spray salt particles explain less than half of the measured salt aerosol particle concentrations in winter, and adding a frost flower particle source improves the agreement substantially (to within 12% of measurements for the cases studied on 1 February 2009). The increase of sodium aerosol mass and total aerosol number concentration due to the addition of sea salt sources from frost flowers is responsible for an increase in cloud droplet number, which enhances cloud optical depth and cloud emissivity. The overall result is a small increase ($0.02\,\mathrm{W\,m^{-2}}$) in downward longwave cloud forcing at the surface. While the increase in sea salt aerosol particle concentration from frost flowers was almost a factor of 2, the effect of this increase on surface warming was negligible.

[24]   While this parameterization used an ad hoc scaling for the magnitude of the emission flux, the spatial distribution and size distribution of emitted salt aerosols from frost flowers were constrained by, respectively, observed source areas (based on satellite retrievals of potential frost flower regions) and measured salt particle size distributions (based on particle size distributions at Barrow). The dependence of this aerosol source on seasonal sea ice formation means that the magnitude and location of this Arctic salt particle source vary as a result of new sea ice formation, making this process coupled between the cryosphere and atmosphere. For instance, a warmer Arctic may reduce wintertime sea ice formation but increase the open water fraction as well as polynyas and leads, which yields more frost flowers and may provide a buffer to the wintertime Arctic aerosols in clean conditions. An Earth system model that incorporates frost flower aerosol emissions in addition to sea ice formation would be needed to explore this possibility. This study provides both a tested source parameterization that can be used in an Earth system model and some initial constraints on the likely magnitude of the cloud and radiative changes expected from salt aerosols emitted from frost flowers during the Arctic winter.

References

Abdul-Razzak, H., and S. J. Ghan (2002), A parameterization of aerosol activation. 3: Sectional representation, *J. Geophys. Res.*, *107*(D3), 4026, doi:10.1029/2001JD000483.

Arctic Climate Impact Assessment (ACIA) (2005), *ACIA Scientific Report*, 1042 pp., Cambridge Univ. Press, Cambridge, U. K. [Available online at www.acia.uaf.edu/pages/scientific.html.]

Alvarez-Aviles, L., W. R. Simpson, T. A. Douglas, M. Sturm, D. Perovich, and F. Domine (2008), Frost flower chemical composition during growth and its implications for aerosol production and bromine activation, *J. Geophys. Res.*, *113*, D21304, doi:10.1029/2008JD010277.

Beaudon, E., and J. Moore (2009), Frost flower chemical signature in winter snow on Vestfonna ice cap (Nordaustlandet, Svalbard), *Cryosphere Discuss.*, *3*, 159–180, doi:10.5194/tcd-3-159-2009.

Bowman, J. S., and J. W. Deming (2010), Elevated bacterial abundance and exopolymers in saline frost flowers and implications for atmospheric chemistry and microbial dispersal, *Geophys. Res. Lett.*, *37*, L13501, doi:10.1029/2010GL043020.

Chen, F., and J. Dudhia (2001), Coupling an advanced land-surface/hydrology model with the Penn State/NCAR MM5 modeling system. Part I: Model description and implementation, *Mon. Weather Rev.*, *129*, 569–585, doi:10.1175/1520-0493(2001)129<0569:CAALSH>2.0.CO;2.

Chou, M. D., M. J. Suarez, C. H. Ho, M. M. H. Yan, and K. T. Lee (1998), Parameterizations for cloud overlapping and shortwave single-scattering properties for use in general circulation and cloud ensemble models, *J. Clim.*, *11*, 202–214, doi:10.1175/1520-0442(1998)011<0202:PFCOAS>2.0.CO;2.

Christner, B. C., C. E. Morris, C. M. Foreman, R. Cai, and D. C. Sands (2008), Ubiquity of biological ice nucleators in snowfall, *Science*, *319*(5867), 1214, doi:10.1126/science.1149757.

Domine, F., A. S. Taillandier, W. R. Simpson, and K. Severin (2005), Specific surface area, density and microstructure of frost flowers, *Geophys. Res. Lett.*, *32*, L13502, doi:10.1029/2005GL023245.

Fenger, M., L. L. Sørensen, K. Kristensen, B. Jensen, Q. T. Nguyen, J. K. Nøjgaard, A. Massling, H. Skov, T. Becker, and M. Glasius (2013), Sources of anions in aerosols in northeast Greenland during late winter, *Atmos. Chem. Phys.*, *13*, 1569–1578, doi:10.5194/acp-13-1569-2013.

Fuentes, E., H. Coe, D. Green, and G. McFiggans (2011), On the impacts of phytoplankton-derived organic matter on the properties of the primary marine aerosol–Part 2: Composition, hygroscopicity and cloud condensation activity, *Atmos. Chem. Phys.*, *11*, 2585–2602, doi:10.5194/acp-11-2585-2011.

Gantt, B., J. Xu, N. Meskhidze, Y. Zhang, A. Nenes, S. J. Ghan, X. Liu, R. Easter, and R. Zaveri (2012), Global distribution and climate forcing of marine organic aerosol–Part 2: Effects on cloud properties and radiative forcing, *Atmos. Chem. Phys.*, *12*, 6555–6563, doi:10.5194/acp-12-6555-2012.

Geever, M., C. D. O'Dowd, S. van Ekeren, R. Flanagan, D. E. Nilsson, G. de Leeuw, and U. Rannik (2005), Submicron sea spray fluxes, *Geophys. Res. Lett.*, *32*, L15810, doi:10.1029/2005GL023081.

Heintzenberg, J., D. C. Covert, and R. Van Dingenen (2000), Size distribution and chemical composition of marine aerosols: A compilation and review, *Tellus, Ser. B*, *52*, 1104–1122.

Hong, S.-Y., and J.-O. J. Lim (2006), The WRF single-moment 6-class microphysics scheme (WSM6), *J. Korean Meteorol. Soc.*, *42*, 129–151.

Houghton, J. T., Y. Ding, D. J. Griggs, M. Noguer, P. J. Van der Linden, X. Dai, K. Maskell, and C. A. Johnson (Eds) (2001), *Climate Change 2001: The Scientific Basis*, 881 pp., Cambridge Univ. Press, Cambridge, U. K.

Iacono, M. J., J. S. Delamere, E. J. Mlawer, M. W. Shephard, S. A. Clough, and W. D. Collins (2008), Radiative forcing by long-lived greenhouse gases: Calculations with the AER radiative transfer models, *J. Geophys. Res.*, *113*, D13103, doi:10.1029/2008JD009944.

Intrieri, J. M., C. W. Fairall, M. D. Shupe, P. O. G. Persson, E. L. Andreas, P. S. Guest, and R. E. Moritz (2002), An annual cycle of Arctic surface cloud forcing at SHEBA, *J. Geophys. Res.*, *107*(C10), 8039, doi:10.1029/2000JC000439.

Janjic, Z. I. (1996), The surface layer in the NCEP Eta Model, paper presented at 11th Conference on Numerical Weather Prediction, Am. Meteor. Soc., Norfolk, Va.

Kaleschke, L., A. Richter, and J. Burrow (2004), Frost flowers on sea ice as a source of sea salt and their influence on tropospheric halogen chemistry, *Geophys. Res. Lett.*, *31*, L16114, doi:10.1029/2004GL020655.

Kalnay, E., et al. (1996), The NCEP/NCAR 40-year reanalysis project, *Bull. Am. Meteorol. Soc.*, *77*, 437–471, doi:10.1175/1520-0477(1996)077<0437:TNYRP>2.0.CO;2.

Khain, A., and A. Pokrovsky (2004), A simulation of effects of atmospheric aerosols on deep turbulent convective clouds using a spectral microphysics mixed-phase cumulus cloud model. Part II: Sensitivity study, *J. Atmos. Sci.*, *61*, 2983–3001.

Li, G., Y. Wang, and R. Zhang (2008), Implementation of a two-moment bulk microphysics scheme to the WRF model to investigate aerosol-cloud interaction, *J. Geophys. Res.*, *113*, D15211, doi:10.1029/2007JD009361.

Lin, Y.-L., R. D. Farley, and H. D. Orville (1983), Bulk parameterization of the snow field in a cloud model, *J. Clim. Appl. Meteorol.*, *22*, 1065–1092, doi:10.1175/1520-0450(1983)022<1065:BPOTSF>2.0.CO;2.

Lubin, D., and A. M. Vogelmann (2006), A climatologically significant aerosol longwave indirect effect in the Arctic, *Nature*, *439*, 453–456.

Mahowald, N. M., J.-F. Lamarque, X. X. Tie, and E. Wolff (2006), Sea salt aerosol response to climate change: Last Glacial Maximum, preindustrial, and doubled carbon dioxide climates, *J. Geophys. Res.*, *111*, D05303, doi:10.1029/2005JD006459.

Martensson, E. M., E. D. Nilsson, G. de Leeuw, L. H. Cohen, and H.-C. Hansson (2003), Laboratory simulations and parameterization of the primary marine aerosol production, *J. Geophys. Res.*, *108*(D9), 4297, doi:10.1029/2002JD002263.

Maslanik, J., and J. Stroeve (1999), Near-real-time DMSP SSM/I-SSMIS daily polar gridded sea ice concentrations, updated daily, 27 January to 2 February 2009, National Snow and Ice Data Center. Digital media, Boulder, Colorado USA.

Ming, Y., and L. M. Russell (2001), Predicted hygroscopic growth of sea salt aerosol, *J. Geophys. Res.*, *106*, 28,259–28,274.

Moore, M. J. K., H. Furutani, G. C. Roberts, R. C. Moffet, M. K. Gilles, B. Palenik, and K. A. Prather (2011), Effect of organic compounds on cloud condensation nuclei (CCN) activity of sea spray aerosol produced by bubble bursting, *Atmos. Environ.*, *45*(39), 7462–7469, doi:10.1016/j.atmosenv.2011.04.034.

Morrison, H., G. de Boer, G. Feingold, J. Harrington, M. D. Shupe, and K. Sulia (2012), Resilience of persistent Arctic mixed-phase clouds, *Nat. Geosci.*, *5*, 11–17, doi:10.1038/ngeo1332.

Nghiem, S. V., D. K. Hall, T. L. Mote, M. Tedesco, M. R. Albert, K. Keegan, C. A. Shuman, N. E. DiGirolamo, and G. Neumann (2012), The extreme melt across the Greenland ice sheet in 2012, *Geophys. Res. Lett.*, *39*, L20502, doi:10.1029/2012GL053611.

Nilsson, E. D., Ü. Rannik, E. Swietlicki, C. Leck, P. P. Aalto, J. Zhou, and M. Norman (2001), Turbulent aerosol fluxes over the Arctic Ocean. 2: Wind-driven sources from the sea, *J. Geophys. Res.*, *106*, 32,139–32,154, doi:10.1029/2000JD900747.

Obbard, R. W., H. K. Roscoe, E. W. Wolff, and H. M. Atkinson (2009), Frost flower surface area and chemistry as a function of salinity and temperature, *J. Geophys. Res.*, *114*, D20305, doi:10.1029/2009JD012481.

Perovich, D. K., and J. A. Richter-Menge (1994), Surface characteristics of lead ice, *J. Geophys. Res.*, *99*, 16,341–16,350, doi:10.1029/94JC01194.

Piot, M., and R. von Glasow (2009), Modelling the multiphase near-surface chemistry related to ozone depletions in polar spring, *J. Atmos. Chem.*, *64*(2–3), 77–105.

Porter, D. F., J. J. Cassano, and M. C. Serreze (2011), Analysis of the Arctic atmospheric energy budget in WRF: A comparison with reanalyses and satellite observations, *J. Geophys. Res.*, *116*, D22108, doi:10.1029/2011JD016622.

Quinn, P. K., T. S. Bates, K. Schulz, and G. E. Shaw (2009), Decadal trends in aerosol chemical composition at Barrow, Alaska: 1976–2008, *Atmos. Chem. Phys.*, *9*, 8883–8888, doi:10.5194/acp-9-8883-2009.

Randles, C. A., L. M. Russell, and V. Ramaswamy (2004), Hygroscopic and optical properties of organic sea salt aerosol and consequences for climate forcing, *Geophys. Res. Lett.*, *31*, L16108, doi:10.1029/2004GL020628.

Rankin, A. M., and E. W. Wolff (2003), A year-long record of size-segregated aerosol composition at Halley, Antarctica, *J. Geophys. Res.*, *108*(D24), 4775, doi:10.1029/2003JD003993.

Rankin, A. M., V. Auld, and E. W. Wolff (2000), Frost flowers as a source of fractionated sea salt aerosol in the polar regions, *Geophys. Res. Lett.*, *27*, 3469–3472, doi:10.1029/2000GL011771.

Rankin, A. M., E. W. Wolff, and S. Martin (2002), Frost flowers: Implications for tropospheric chemistry and ice core interpretation, *J. Geophys. Res.*, *107*(D23), 4683, doi:10.1029/2002JD002492.

Roscoe, H. K., B. Brooks, A. V. Jackson, M. H. Smith, S. J. Walker, R. W. Obbard, and E. W. Wolff (2011), Frost flowers in the laboratory: Growth, characteristics, aerosol, and the underlying sea ice, *J. Geophys. Res.*, *116*, D12301, doi:10.1029/2010JD015144.

Rosenfeld, D. (1999), TRMM observed first direct evidence of smoke from forest fires inhibiting rainfall, *Geophys. Res. Lett.*, *26*, 3105–3108.

Russell, L. M., L. N. Hawkins, A. Frossard, P. Quinn, and T. Bates (2010), Carbohydrate-like composition of submicron atmospheric particles and their production from ocean bubble bursting, *Proc. Natl. Acad. Sci. U. S. A.*, *107*(15), 6652–6657, doi:10.1073/pnas.0908905107.

Shaw, P. M., L. M. Russell, A. Jefferson, and P. K. Quinn (2010), Arctic organic aerosol measurements show particles from mixed combustion in spring haze and from frost flowers in winter, *Geophys. Res. Lett.*, *37*, L10803, doi:10.1029/2010GL042831.

Simpson, W. R., D. Carlson, G. Hönninger, T. A. Douglas, M. Sturm, D. Perovich, and U. Platt (2007), First-year sea-ice contact predicts bromine monoxide (BrO) levels at Barrow, Alaska better than potential frost flower contact, *Atmos. Chem. Phys.*, *7*, 621–627, doi:10.5194/acp-7-621-2007.

Style, R. W., and M. G. Worster (2009), Frost flower formation on sea ice and lake ice, *Geophys. Res. Lett.*, *36*, L11501, doi:10.1029/2009GL037304.

Westervelt, D. M., R. H. Moore, A. Nenes, and P. J. Adams (2012), Effect of primary organic sea spray emissions on cloud condensation nuclei concentrations, *Atmos. Chem. Phys.*, *12*, 89–101, doi:10.5194/acp-12-89-2012.

Xie, S., et al. (2010), Clouds and more: ARM climate modeling best estimate data, *Bull. Am. Meteorol. Soc.*, *91*, 13–20, doi:10.1175/2009BAMS2891.1.

Yang, X., J. A. Pyle, and R. A. Cox (2008), Sea salt aerosol production and bromine release: Role of snow on sea ice, *Geophys. Res. Lett.*, *35*, L16815, doi:10.1029/2008GL034536.

Zaveri, R. A., and L. K. Peters (1999), A new lumped structure photochemical mechanism for large-scale applications, *J. Geophys. Res.*, *104*, 30,387–30,415.

Zaveri, R. A., R. C. Easter, J. D. Fast, and L. K. Peters (2008), Model for Simulating Aerosol Interactions and Chemistry (MOSAIC), *J. Geophys. Res.*, *113*, D13204, doi:10.1029/2007JD008782.

Zhao, T. L., S. L. Gong, J. W. Bottenheim, J. C. McConnell, R. Sander, L. Kaleschke, A. Richter, A. Kerkweg, K. Toyota, and L. A. Barrie (2008), A three-dimensional model study on the production of BrO and Arctic boundary layer ozone depletion, *J. Geophys. Res.*, *113*, D24304, doi:10.1029/2008JD010631.